RSC Advances

PAPER

View Article Online
View Journal | View Issue

Cite this: *RSC Adv.*, 2019, **9**, 16223

Nonlinear optical behavior of n-tuple decker phthalocyanines at the nanosecond regime: investigation of change in mechanisms†

Kutloano E. Sekhosana ‡* and Tebello Nyokong ‡*

The coordination system of rare-earth n-tuple decker phthalocyanines would be better suited with appropriate metal ions with the correct coordination number and the solvent system of the reaction, amongst other reasons, for the formation of n-tuple decker phthalocyanines. As a result, these complexes are very rare. In this manuscript, we present new n-tuple decker phthalocyanines in the form of double- (complex **2**), quadruple- (complex **3a**) and sextuple-decker phthalocyanines (complex **3b**), all of which contain neodymium and cadmium metal ions. The primary focus is the investigation of the nonlinear optical (NLO) mechanisms responsible for the observed reverse saturable absorption. While the extension of the π-electron system has been found to enhance the nonlinear optical behavior of complexes **3a** and **3b**, a change in the NLO mechanisms has been observed, with complex **2** lacking the triplet state population, as revealed by a laser flash photolysis technique. It has also been established that the excited state absorption cross sections follow a clear order of magnitude for the complexes under investigation: σ_{23} (for **3b**) > σ_{23} (for **3a**) > σ_{1m} (for **2**). This trend evidences the effects of the extension of the π-electron system.

Received 11th March 2019
Accepted 25th April 2019

DOI: 10.1039/c9ra01836k

rsc.li/rsc-advances

1. Introduction

Macroheterocyclic tetraazoporphyrin ring complexes can be modified in such a way that the ligands interact with each other *via* coordination to transition metals and/or lanthanide ions, as is the case with multi-decker phthalocyaninato molecules. Such complexes are also referred to as advanced materials[1] and find applications in many fields as single-molecule magnets,[2–10] sensors,[11–13] conductive materials,[14–17] optical limiters,[18–28] ambipolar organic field-effect transistors,[29,30] supramolecular spin valves[31] and self-assembled nanostructures.[32,33] Lanthanide double-decker phthalocyanine ($LnPc_2$) complexes, in particular, have been the center of interest in research for a long time.[26,34] However, new developments have paved the way for the discovery of even more complex materials in the form of triple-decker,[35] quadruple-decker,[36] quintuple-decker[37] and a sextuple-decker phthalocyanines.[38] The sextuple-decker, to the best of our knowledge, has been prepared once. Therefore, it can be concluded that not much has been done in terms of developing such materials. The scarcity of such structures has been attributed to the selection of an appropriate metal ion with the necessary coordination number, geometry, charge, and hard/soft-acid/base characteristics to suit the coordination algorithm of tetrapyrroles.[37] For simplicity, all sandwich-type phthalocyaninato complexes, presented in this manuscript, are termed n-tuple decker phthalocyaninato molecules. Quandruple-decker phthalocyaninato molecules have not been investigated for optical limiting, while their sextuple-decker counterparts have been shown to possess good optical limiting properties.[37] This manuscript narrows its focus on investigating the mechanisms governing the reverse saturable absorption as well as the effects of π-conjugation on the optical limiting properties of the new n-tuple decker phthalocyanines in solution and thin films. These molecules are based on neodymium and cadmium metal ions. The bulk *tert*-butyl phenoxy substituents enhance the solubility in nonpolar solvents, hence the choice of dichloromethane as the solvent medium. All the molecules presented in this manuscript are new, since the *tert*-butyl phenoxy substituted n-tuple decker phthalocyanines have not been reported elsewhere. The molecules are embedded in polymers to form thin films for nonlinear optical (NLO) limiting studies. Poly(bisphenol A carbonate) was selected as the polymer for thin films because of its superior solubility in nonpolar solvents, thereby, limiting the challenges of the manufacturing of thin films.

2. Experimental

2.1 Materials

Deuterated chloroform ($CDCl_3$), 1-pentanol, 1,2,4-trichlorobenzene (TCB), and neodymium(III) acetate hydrate were purchased from Sigma-Aldrich. Dimethyl formamide (DMF), chloroform and

---

Institute for Nanotechnology and Innovation, Department of Chemistry, Rhodes University, PO Box 94, Grahamstown 6140, South Africa. E-mail: sekhosanake@gmail.com; t.nyokong@ru.ac.za

† Electronic supplementary information (ESI) available: NMR spectra of complexes **2** and **3a**, mass spectra **3a** and **3b**, ESR spectra of **2**, **3a** and **3b**, and SEM images of **2-TF**, **3a-TF** and **3b-TF**. See DOI: 10.1039/c9ra01836k

‡ These authors contributed equally.

dichloromethane (DCM) were purchased from MINEMA. Cadmium acetate dihydrate, 1,8-diazabicyclo[5.4.0]undec-7-ene (DBU) and poly(bisphenol A) carbonate were purchased from Fluka. Water was obtained from Milli-Q Water Systems (Millipore Corp., Bedford, MA, USA). The synthesis of bis-{2(3),9(10),16(17),23(24)-tetra(4-*tert*-buylphenoxy) phthalocyaninato} neodymium(III) (**2**) was reported in our previous publication.[39]

2.2 Synthesis of quadruple-decker phthalocyanine (3a) (Scheme 1)

Complex **2** (40 mg; 16.99 μmol) was placed in a clean round bottom flask (50 mL) that contained cadmium acetate hydrate (4.36 mg; 16.34 μmol). TCB (6 mL) was added to the reaction mixture under a blanket of argon, followed by refluxing for 24 h. Next, TCB was evaporated and the crude product was cooled to room temperature. The mixture of ethanol and water (v/v 1 : 1) was used for further purification under centrifugation at 3000 rpm before the oven-dried blue product was loaded onto a chromatography column packed with silica. A $CHCl_3$ and *n*-hexane solvent mixture was first used to remove the unreacted complex **2**, after which a $CHCl_3$ and methanol mixture (v/v 14 : 1) was employed to elute complex **3a** as the second band, which was dried in open air. Yield: (67%). IR: [KBr, ν, cm^{-1}] 748, 771, 886, 940, 1013 (*Pc* skeleton), 1040, 1074, 1107, 1173, 1228, 1254 (C–O–C), 1326, 1363, 1392, 1471, 1506, 1600, 1737 (benzene, pyrrole, isoindole and aza), 2866, 2922, 2956 (C–H). UV-Vis (DCM): λ_{max}-nm (log ε), 336 (4.79), 640 (4.85). Anal. calc. for $C_{288}H_{256}N_{32}O_{16}$-$Nd_2Cd$: C, 71.73; H, 5.35; N, 9.29%. Found: C, 71.66; H, 5.21; N, 9.32%. ^1H NMR ($CDCl_3$) for **3a** δ, ppm 7.40–7.30 (18H, m, H-Ar), 7.14–6.96 (34H, m, H-Ar), 6.78–6.74 (20H, m, H-Ar), 6.47–6.34 (24H, m, H-Ar), 5.98 (16H, m, H-Ar), 1.49 (22H, m, H-*t*Bu), 1.30–1.27 (34H, m, H-*t*Bu), 1.08–1.05 (17H, H-*t*Bu), 1.01–0.98 (33H, m, H-*t*Bu), 0.86–0.77 (38H, m, H-*t*Bu). MS (MALDI-TOF): (*m*/*z*): calc. 4822 amu. Found: 4824 amu $[M + 2H]^+$.

2.3 Synthesis of sextuple-decker phthalocyanine (3b) (Scheme 1)

Complex **3b** was obtained as a by-product from the same reaction as that of complex **3a**, except that a $CHCl_3$ and methanol mixture (v/v 9 : 1) was used for the elution of the third blue band containing the required product. Yield: (22%). IR: [KBr, ν, cm^{-1}] 722, 747, 824, 886, 939, 1013 (*Pc* skeleton), 1041, 1074, 1106, 1173, 1229, 1254, 1289 (C–O–C), 1328, 1363, 1393, 1465, 1507, 1601, 1730 (benzene, pyrrole, isoindole and aza), 2852, 2922, 2954 (C–H). UV-Vis (DCM): λ_{max} nm (log ε), 338 (4.98), 636 (5.08). Anal. calc. for $C_{432}H_{384}N_{48}O_{24}Nd_3Cd_2$: C, 71.18; H, 5.94; N, 9.22%. Found: C, 71.09; H, 6.11; N, 9.26%. ^1H NMR ($CDCl_3$) for **3b**: δ, ppm 7.79–7.71 (26H, m, H-Ar), 7.47–7.24 (42H, m, H-Ar), 7.13–6.93 (51H, m, H-Ar), 6.43–5.63 (49H, m, H-Ar), 1.53–1.35 (72H, m, H-*t*Bu), 1.29 (6H, s, H-*t*Bu), 1.26 (8H, s, H-*t*Bu), 1.21 (7H, s, H-*t*Bu), 1.07–0.94 (63H, m, H-*t*Bu), 0.83–0.76 (60H, m, H-*t*Bu). MS (MALDI-TOF): (*m*/*z*): calc. 7290 amu. Found: 7291 amu $[M + H]^+$.

2.4 Preparation of thin films

Using **3b** and **3c**, thin films (**3b-TF** and **3c-TF**) were obtained by following the procedure for the synthesis of the corresponding thin film formed from complex **2** (ref. 39) at the same concentrations (3.0×10^{-4} M). The thickness of the film was measured to be ~6 μm using the knife edge attachment of the Bruker D8 Discover X-ray diffraction (XRD) diffractometer.

2.5 Equipment

Infrared spectra were recorded on a Perkin Elmer 100 ART FT-IR spectrometer. Ultraviolet-visible (UV-Vis) spectra were recorded on a Shimadzu UV-Vis 2550 spectrophotometer. Emission spectra were recorded on a Varian Cary Eclipse fluorescence spectrophotometer. Luminescence lifetime measurements were performed using time correlated single photon counting setup (TCSPC) (PicoQuant FluoTime 300). The excitation source was a diode laser (LDH-P-C-485, 480 nm, 10 MHz repetition rate, 44 ps pulse width, Picoquant GmbH). The details were provided previously.[40,41]

^1H NMR studies were performed using a Bruker AMX 600 NMR spectrometer. Elemental analysis experiments were carried out on a Vario-Elementar Microcube ELIII. Mass spectral data were collected using a Bruker AutoFLEX III Smart beam TOF/TOF Mass spectrometer. The spectra were acquired using α-cyano-4-hydroxycinnamic acid as the MALDI matrix and a 355 nm Nd:YAG laser as the ion source.

Electron spin resonance (EPR) spectra were recorded on a Bruker EPR 300E X-band (10 GHz) spectrometer equipped with a TM probe with ESR tubes. The spin Hamiltonian parameters were obtained by the simulation of the spectra. The static field (2500 G), center field (3500 G), modulation amplitude (100 G), sweep time (20.97 ms), time constant (10.24 ms), conversion time (5.12 ms), resolution (2048 pts), power (2.00 mW) and modulation frequency (100 kHz) were used as the experimental parameters at 298 K with 10 scans. Scanning electron microscope (SEM) images of thin films (**2-TF**, **3a-TF**, and **3b-TF**) were obtained using a JOEL JSM 840 scanning electron microscope operated at 20 kV.

X-ray powder diffraction patterns were recorded on a Bruker D8 Discover equipped with a proportional counter, using Cu-K_α radiation ($\lambda = 1.5405$ Å, nickel filter). The details were reported previously.[40,41]

All *Z*-scan experiments described in this study were performed using a frequency-doubled Nd:YAG laser (Quanta-Ray, 1.5 J/10 ns fwhm pulse duration) as the excitation source. A standard quartz cuvette with a lid (0.2 cm), purchased from Purshee, was used for the experiments performed in solution. Details were provided previously.[18,42]

3. Results and discussion

3.1 Synthesis of n-tuple decker phthalocyaninato complexes and their respective thin films

The conversion of $LnPc_2$ complexes into stable quadruple-decker phthalocyanines is achieved by employing cadmium salts in the presence of TCB at reflux temperature.[36] Similar methods have been employed to design sextuple-decker phthalocyanines[38] using unmetallated phthalocyanine (H_2Pc). Following these methods and placing complex **2** and cadmium acetate dehydrate in the TCB bath at reflux temperature, complexes **3a** and **3b** were formed. This is the first time when quadruple- and sextuple-decker phthalocyanines were synthesized in the same reaction vessel. It is also the first time when a sextuple-decker phthalocyanine was obtained by sandwiching two Cd(II) ions between three $LnPc_2$ complexes. The contributing factors to this can be thought of as the mole ratio of complex **2** to the cadmium ion and time. However, the yield of 67% for complex **3a** is desirable, considering that complex **3b** is simultaneously formed. Separation of such highly stable complexes is, therefore, challenging.

Complexes **2**, **3a** and **3b** dissolve in highly volatile nonpolar solvents such tetrahydrofuran, chloroform and dichloromethane, as is the case with poly(bisphenol A) carbonate. For the preparation of thin films, chloroform was chosen as the best solvent with a controllable rate of evaporation.

3.2 Structural characterization of $LnPc_2$ complexes and their respective thin films

3.2.1 Vibrational spectroscopy. Complex **2** shows the $Pc^{\bullet -}$ IR marker at 1313 cm^{-1}. A similar observation has been reported where an $LnPc_2$ complex showed a $Pc^{\bullet -}$ IR marker, while the quadruple-decker *Pc* did not have this marker.[43] This difference in the vibrational frequencies of complexes **3a** and **3b** with respect to that of **2** is very important and characterizes a complete structural change and the nature of complexes under investigation. The core of the *Pc* skeleton is characterized by vibrational bands located between ~700 and 1050 cm^{-1}. These bands were observed in the range of 722–1041 cm^{-1} for complexes **2**, **3a** and **3b**. The C–O–C vibrations, characterizing the link between the benzene ring of the *Pc* core and the *tert*-butyl benzene of the substituent, were observed between 1074 and 1228 cm^{-1}. The other vibrational characteristics of the three complexes are the C=C, C=N– and C–N moieties of the benzene ring, azo and the isoindole groups. These vibrations were observed between 1326 and 1601 cm^{-1} for complexes **2**, **3a** and **3b**. The *tert*-butyl and C–H vibrations of the *tert*-butyl benzene or the benzene rings of these complexes appeared at ~2852 to 2954 cm^{-1}. It was observed that complex **2** absorbed moisture (Fig. 1), which was characterized by the OH– stretch at 3481 cm^{-1}.

3.2.2 Proton nuclear magnetic resonance spectroscopy. ^1H NMR signals for complexes **2**, **3a** and **3b** were obtained in $CDCl_3$ at room temperature. Complex **2** showed two broad aromatic proton (H-Ar) bands in the ranges of 7.57–7.00 and 6.01–5.68 ppm, complemented by the *tert*-butyl proton signals (H-*t*Bu) found at 1.59–0.65 ppm. Complex **3a** showed broad signals between 7.40–5.98 ppm, indicative of aromatic protons. Aliphatic protons were characterized by signals between 1.49–0.77 ppm, as would be expected for protons of the *tert*-butyl groups. For complex **3b**, aromatic protons were found in the range of 7.79–5.63 ppm, while *tert*-butyl protons were found in the range of 1.53–0.76 ppm. In general, ^1H NMR signals of the three complexes represented the correct number of expected protons corresponding to the predicted structures. Fig. S1† shows the ^1H NMR signatures for complexes **2** and **3a** as examples.

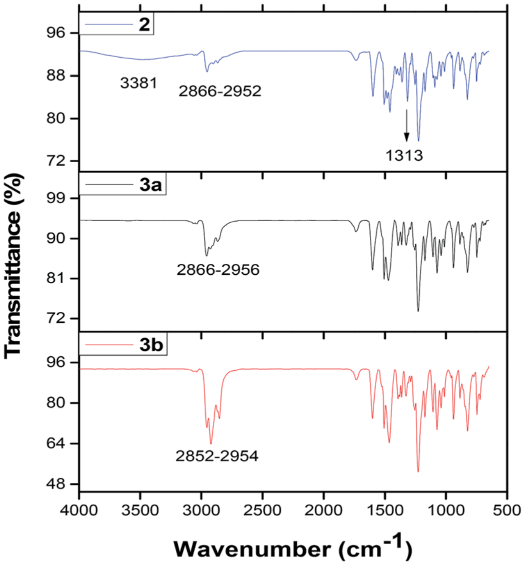

Fig. 1 FTIR spectra of complexes **2**,[39] **3a** and **3b**.

3.2.3 Mass spectrometry. Complex **2** was the primary material from which complexes **3a** and **3b** were formed. Therefore, the comparison of the masses of these complexes is very important and helps to elucidate the structural differences. As a primary material, complex **2** is less bulky than complexes **3a** and **3b**, with **3b** being the bulkiest. The mass of complex **2** has been reported before.[39] For complexes **3a** and **3b**, 4822 and 7290 amu were the expected masses, respectively. These experimentally determined masses correspond well with the structures of the complexes **3a** and **3b** whose theoretical masses are 4824 and 7291 amu, respectively (Fig. S2†).

3.2.4 Absorption spectroscopy. Neutral $LnPc_2$ complexes are characterized by a complicated system of ground state electronic transitions which are forbidden in the idealized D_{4h} or D_{4d} symmetry,[43–46] resulting in various absorption bands. The B-band (at 326 and 365 nm) for complex **2** in DCM (Fig. 2) was split, while the blue valence (BV)[47–50] and the Q-bands (485 and 690 nm, respectively) were also observed. The absorption spectrum of complex **2** has been discussed in detail before.[39] For complexes **3a** and **3b**, the Q-band appeared to be more blue-

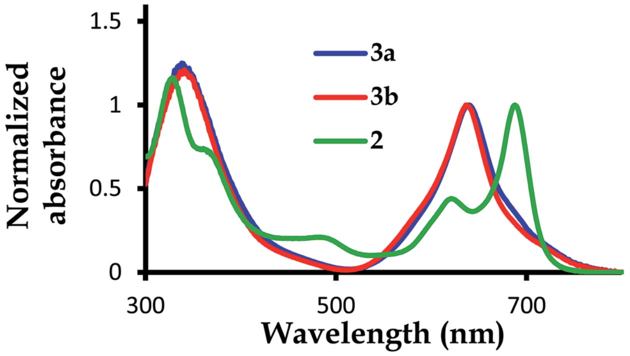

Fig. 2 The normalized UV-Vis absorption spectra for complexes **2**,[39] **3a** and **3b**, with **2** showing a blue valence band when the Q-bands for **3a** and **3b** are blue shifted with no blue valence band observed.

shifted (Fig. 2) to about 640 and 636 nm, respectively, with the complete disappearance of the BV band. The absorption spectra of complexes **3a** and **3b** are also similar to those of other quadruple- and sextuple-decker phthalocyanines. In general, the absorption spectrum of complex **2** is similar to the spectra of other $LnPc_2$ complexes[19,25,51,52] and resembles the energy diagram that manipulates the electronic transitions in accordance with the Valence-Effective Hamiltonian (VEH) calculation,[53] where the Q-band is attributed to the electronic transitions from the $\pi(a_{2u})$ to the $\pi^*(e_g^*)$ orbitals.

The B-band results from the transitions between $\pi(b_{2u})$ and $\pi^*(e_g^*)$.[51,52] The absorption spectra of complexes **3a** and **3b** are broader than those of blue forms[39] but comparable to those of similar analogues.[38]

3.2.5 Electron spin resonance spectroscopy. The $LnPc_2$ complexes are characterized by π-radical related electronic transitions that imply imbalance in the number of electrons in two coordinating *Pc* entities, given the 3+ oxidation state of lanthanide ions. In this case, one *Pc* ring would have two electrons and the other would have one, having the formulation ($Pc(-2)Nd^{III}Pc(-1)$). Electron spin resonance (ESR) is, therefore, an efficient technique to manipulate data that depicts the behavior of the moving unpaired electrons in a molecule. For complex **2**, an ESR band was observed at ~3487 to 3496 G with two hyperfines at ~3482 and 3521 G at $g = 2.000$ in solid state (Fig. S3†). This observation is in agreement with the behavior of $LnPc_2$ complexes which are regarded as single-hole complexes, in which an unpaired electron is present in one of the macrocyclic ligands,[54] formulated as $Pc(-2)Ln^{III}Pc(-1)$. The ESR bandwidth of complex **2** at 298 K is ~8.01 G, which is broader than the bands of the other neodymium based phthalocyanines.[55] The ESR spectroscopy data for complex **2** was reported earlier[39] and is provided in Fig. S3.†

When the emergence of the ESR band is governed by the movement of an unpaired electron originating directly from the π-radicals, it would be expected that a phthalocyanine molecule, obtained *via* modification of a neutral $LnPc_2$ complex, should not exhibit an ESR signal. However, for complexes **3a** and **3b**, ESR bands were observed. These ESR signals were characterized by intensities much higher than that of complex **2**. Even though complexes **3a** and **3b** lack π-radicals, the presence of paramagnetic neodymium ions can encourage the movement of electrons. Since there are more paramagnetic neodymium ions in complexes **3a** and **3b** than in complex **2** (Fig. S3†), the presence of ESR signals of higher intensity is not surprising.

3.2.6 X-ray diffractometry. The X-ray diffractograms of complex **2** and its corresponding thin film (**TF-2**) have been reported before[39] and are shown in Fig. 3 for comparison. Similar patterns were observed for complexes **3a** and **3b** and their corresponding thin films (**3a-TF** and **3b-TF**).

The only difference between X-ray diffractograms of the films is an additional sharp XRD peak observed at 38° only for **2-TF**. The overall change in the XRD pattern signifies the influence of poly(bisphenol A) carbonate on the complex. The sizes of complexes **2**, **3a** and **3b** were determined using the Debye–Scherrer equation[56] to fit the XRD diffractograms and found to be 0.81, 1.56 and 1.87 nm, respectively.

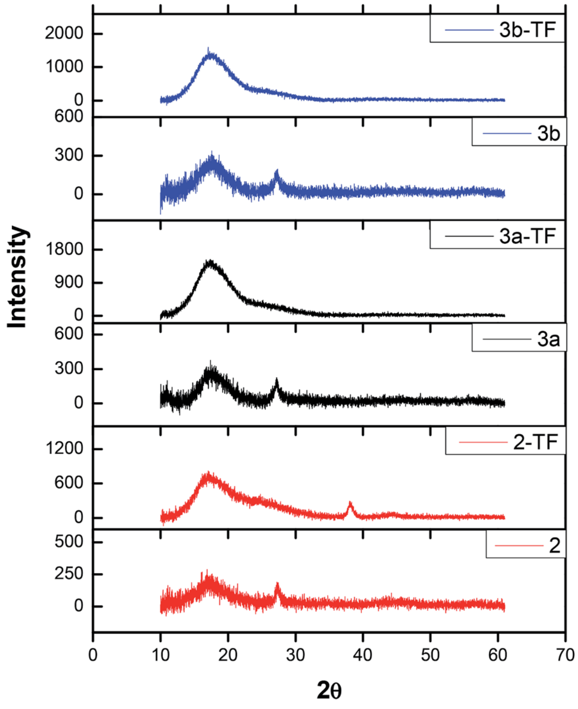

Fig. 3 X-ray diffractograms of complexes **2**,[39] **3a** and **3b** in powder form as well as their respective thin films **2-TF**,[39] **3a-TF** and **3b-TF**.

3.3 Nonlinear optical signatures

The nonlinear optical behavior of a material can be monitored by subjecting the material to highly illuminating laser beams. The behavior is then analyzed as the material moves along the *z*-axis through the focal point of converging irradiation using the *Z*-scan technique. The intensity modulation affects the material as it approaches the focal point and, therefore, attenuates the transmittance (herein referred to as the normalized transmittance or T_{Norm}). The *Z*-scan is only affected by the nonlinear absorption[22] as all the transmitted light is detected. There are two techniques to detect the transmitted light, namely, the closed aperture and the open aperture *Z*-scans. This manuscript strictly focuses on presenting the data obtained from the open aperture *Z*-scan experiments performed in solution and solid state.

The nonlinear optical parameters for complex **2** and its corresponding thin film (**TF-2**) have been discussed in detail before.[39] For precise comparison of the nonlinear behavior, all the complexes were subjected to the same experimental conditions in the nanosecond regime. The establishment of the reverse saturable absorption (RSA), characterized by the reduction of T_{Norm} at focus ($z = 0$), was achieved upon scanning along the *z*-axis of the *Z*-scan under resonant conditions. This behavior is illustrated for complexes **2**, **3a** and **3b** in Fig. 4A and B.

As can be seen in Fig. 4, the signature only attenuates about 48% of the input fluence for complex **2** as already discussed

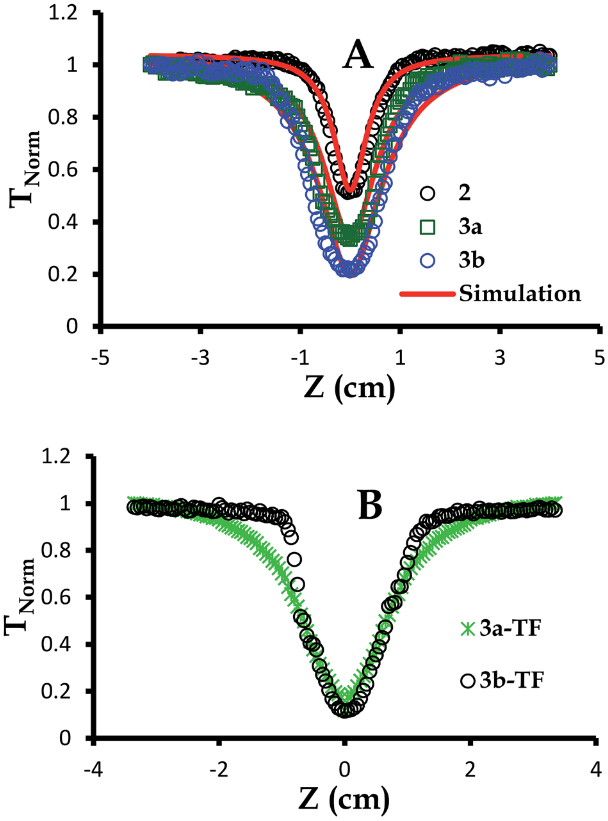

Fig. 4 Open aperture *Z*-scan signatures of (A) **2**,[39] **3a** and **3b** in DCM at 3.0×10^{-4} M and (B) **3a-TF** and **3b-TF**. The simulations were performed employing eqn (6)–(12).

previously.[39] For simplicity and better understanding of the behavior of this complex, we employed an excited state energy diagram similar to that obtained for $\mathrm{LuPc_2}$ by Orti *et al.*, acquired by performing Valence Effective Hamiltonian (VEH) calculations,[44,53] Fig. 5A.

This is the strategy, illustrating that the excited molecules at a_{2u} level undergo the $a_{2u} \rightarrow e_g^*$ electronic transition when the energy is being pumped into level a_{2u}. This electronic transition is depicted by the three-energy level diagram (Fig. 5B) describing similar electronic transitions where the ground singlet state, the first singlet excited state and the higher energy singlet state are denoted by S_0, S_1 and S_m, respectively. With S_0, S_1 and S_m corresponding to e_g, a_{2u} and e_g^*, respectively, the electronic transitions $e_g \rightarrow a_{2u}$ and $a_{2u} \rightarrow e_g^*$ may describe the transition rates w_{01} and w_{1m}, respectively. The excited molecules may relax *via* the relaxation pathways $S_m \rightarrow S_1$ (with decay time τ_{m1}) and $S_1 \rightarrow S_0$ (with the first excited state lifetime τ_{10}). When tuning the energy pump at $e_g \rightarrow a_{2u}$ (by transition rate w_{01} which is around the BV band (*i.e.*, at 532 nm), the molecules at a_{2u} would get excited to e_g^* (S_m level) by the transition rate w_{1m}. The relaxation then takes through $e_g^* \rightarrow a_{2u}(S_m \rightarrow S_1)$ and $a_{2u} \rightarrow e_g$ ($S_1 \rightarrow S_0$) upon losing the photon energy ($h\nu$) *via* τ_{m1} and τ_{10}. At both excitation regions, shown in Fig. 5B, the fractions of molecules at each level can be described using the following laser rate equations[57,58] at $E = 55 \pm 0.1$ μJ:

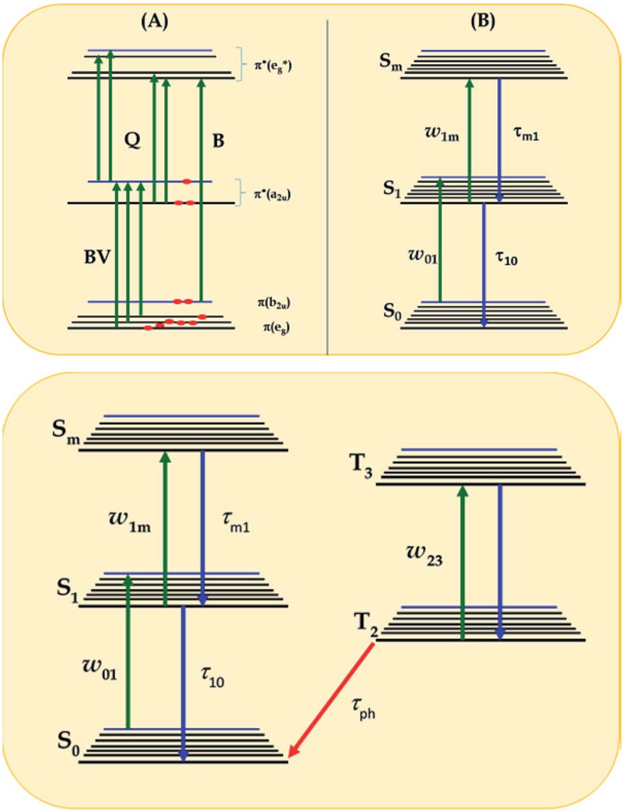

Fig. 5 (A) Diagram showing singlet excited states of $\mathrm{LnPc_2}$ in comparison to that obtained by Orti *et al.* using Valence Effective Hamiltonian calculations;[44,53] (B) three-energy-level diagram used to model the excited state cross-section spectrum within the rate equation model of eqn (1)–(3), according to ref. 56 and 57; and (C) general five-energy level diagram employed for the simulation of the NLO mechanisms of complexes **3a**, **3b**, **3a-TF** and **3b-TF** using eqn (6)–(12).

$$\frac{\mathrm{d}n_0}{\mathrm{d}t} = -w_{01}n_0 + \frac{n_1}{\tau_{10}}, \tag{1}$$

$$\frac{\mathrm{d}n_1}{\mathrm{d}t} = +w_{01}n_0 - w_{1m}n_1 - \frac{n_1}{\tau_{10}} + \frac{n_m}{\tau_{m1}}, \tag{2}$$

$$\frac{\mathrm{d}n_m}{\mathrm{d}t} = +w_{1m}n_1 - \frac{n_m}{\tau_{m1}} \tag{3}$$

In these eqns, n_i is the population fraction of the state ($i = 0$, 1 and m) with $n_0 + n_1 + n_m = 1$; $w_{01} = \sigma_{01}I(t)/h\nu$ and $w_{1m} = \sigma_{1m}I(t)/h\nu$, where σ_{01} and σ_{1m}, are the ground and the singlet excited state absorption cross-sections, respectively, corresponding to the ground state (w_{01}) and the excited state (w_{1m}) transitions; τ_{m1} and τ_{10} are the relaxation lifetimes from the highest excited singlet state (S_m) to the first excited singlet state (S_1) and from the singlet excited state (S_1) to the ground state (S_0), respectively. Eqn (1)–(3) can be numerically solved by considering a GAUSSIAN temporal profile for the laser pulse, with the temporal dependence of the absorption coefficient described by eqn (4):

$$\alpha(t) = N\{n_0(t)\sigma_{01} + n_1(t)\sigma_{1m}\} \quad (4)$$

In eqn (4), N is the sample concentration in molecules per cm^3. For all complexes, N was kept constant at 1.869×10^{17} molecules per cm^3. This concentration is lower than the one reported for the $\mathrm{YbPc_2}$ complex.[57] To calculate the transmittance, the propagation equation, $\mathrm{d}I(t)/\mathrm{d}z(t) = -\alpha(t)I(t)$, can be integrated over the sample thickness L and the full pulse width (t from $-\infty$ to $+\infty$). The ground state cross section is described by eqn (5):[58]

$$\sigma_{01} = \frac{\alpha_{01}}{N} \quad (5)$$

with the linear absorption coefficient, α_{01}, obtained from resonant conditions at 532 nm of the absorption spectrum of the complex under investigation. This model is applicable to $\mathrm{LnPc_2}$ complexes that exhibit no triplet state population.

However, for the sandwich-type phthalocyanes[25] whose triplet population is not affected by ligand–ligand interactions, the singlet excited state may be infinitesimally weaker and the relaxation decay time is far smaller than the laser pulse rate. In this case, a general five-level model (Fig. 5C) can be applied.[59] This model ignores the vibrational levels of the electronic states such that the laser pulse width is assumed to be longer than any relaxation decay times associated with the levels. To further simplify the model, it is assumed that relaxation from S_m and T_3 is very fast,[59] hence the neglection of these two levels. Excitation at 532 nm leads to the S_1 population. As highlighted above, even if the electrons undergo $S_1 \rightarrow S_m$, S_m lifetime is very fast. Therefore, the $S_1 \rightarrow T_2$ transition (τ_{isc}) occurs *via* intersystem crossing (ISC). Once T_2 is populated, the electrons undergo $T_2 \rightarrow T_3$ transition and then relax back to T_2 *via* the $T_3 \rightarrow T_2$ electronic transition. For complexes **3a** and **3b**, the relaxation decay time (τ_{ph}) at T_2 was measured using the laser flash photolysis technique[18] and found to be in the order of microseconds. Using laser flash photolysis, the triplet decay curves for complexes **3a** and **3b** were recorded (Fig. S4†) and fitted. The obtained triplet lifetimes ranged from 27 to 22 μs for complexes **3a** and **3b**, respectively. These values are consistent with the proposed τ_{ph},[59] which has to be much longer than τ_{isc}. Ignoring the stimulated emission from S_1 due to small fluorescence quantum yield, the following modified laser rate equations can be applied to simulate the excitation and relaxation of the system:

$$\frac{\mathrm{d}n_0}{\mathrm{d}t} = -w_{01}n_0 + \frac{n1}{\tau_{10}} + \frac{n_2}{\tau_{ph}}, \quad (6)$$

$$\frac{\mathrm{d}n_1}{\mathrm{d}t} = +w_{01}n_0 - \frac{n_1}{\tau_{\mathrm{isc}}} - \frac{n_1}{\tau_{10}}, \quad (7)$$

$$\frac{\mathrm{d}n_2}{\mathrm{d}t} = +\frac{n_1}{\tau_{\mathrm{isc}}} - \frac{n_2}{\tau_{\mathrm{ph}}} \quad (8)$$

where n_2 refers to the population of T_2. In this model, the luminescence lifetimes ranging from $\tau_{10} = 4.50$ ns to 5.40 ns (Table 1), obtained at 532 nm using the TCSPC technique, were used. The kinetic decay curves for the luminescence lifetimes of complex **2** and its blue form analogues were reported before[39] and those of complexes **3a** and **3b** are shown Fig. S5.† These kinetic decay curves show a good simulation (in red) with the chi-square goodness of fit ranging between 0.998 and 0.999. The propagation equation governs the attenuation of the laser beam with the absorption coefficient including the excited-state absorption from S_1 to T_2:

$$\frac{\mathrm{d}I(t)}{\mathrm{d}z} = -\alpha I(t) = -[\sigma_{01}n_0 + \sigma_{1m}n_1 + \sigma_{23}n_2]I(t), \quad (9)$$

where the triplet state absorption cross section, σ_{23}, is given by $w_{23} = \sigma_{23}I(t)/h\nu$ with w_{23} being the $T_2 \rightarrow T_3$ transition rate.

Under the steady-state approximation, governed by the pulse width much longer than the relaxation time,[60] all the time derivatives are set to zero. The assumption is valid for nanosecond pulses, in the case of phthalocyanines with singlet lifetime in the order of picoseconds.[61] Once eqn (9) has been solved, the intensity-dependent absorption coefficient becomes:

$$\alpha(I(t)) = \frac{\alpha_0}{1 + \dfrac{I(t)}{I_{\mathrm{sat}}}}\left[1 + \frac{\sigma_{1m}}{\sigma_{23}}\frac{\tau_{\mathrm{isc}}}{\tau_{\mathrm{ph}}}\frac{I(t)}{I_{\mathrm{sat}}} + \frac{\sigma_{23}}{\sigma_{01}}\frac{I(t)}{I_{\mathrm{sat}}}\right], \quad (10)$$

where $I_{\mathrm{sat}} = h\nu/\sigma_{01}\tau_{10}$, noting that σ_{23} and σ_{1m} are probably of the same order when $\tau_{\mathrm{isc}} \lll \tau_{\mathrm{ph}}$, and as the triplet yield approaches unity for phthalocyanines, the term can be eliminated with σ_{1m} in the numerator.[59] The five-level model can therefore be effectively reduced to a three-level model with the intensity-dependent absorption coefficient given by:

$$\alpha(I(t), I_{\mathrm{sat}}, k) = \frac{\alpha_0}{1 + \dfrac{I(t)}{I_{\mathrm{sat}}}}\left[1 + k\frac{I(t)}{I_{\mathrm{sat}}}\right], \quad (11)$$

where the excited-state absorption cross section is due to σ_{23}; in this case, $k = \sigma_{23}/\sigma_{01}$. It can be noted that there is a direct relationship between $I(t)$ and the pulse energy density (given as $F = E_{\mathrm{Pulse}}/\pi w(z)^2$), with E_{Pulse} being the energy per unit pulse and $\pi w(z)^2$ defining the surface area through which the pulse propagates at position z. In eqn (9), $I(t)/I_{\mathrm{sat}}$ can, therefore, be replaced by the pulse energy density per unit energy density saturation F/F_{sat}. The latter is defined at the output saturation of the energy density pulse.

High k and β_{eff}, low F_{sat} and low α_0 values are characteristic of a superior optical limiter.[50] The value of $\alpha(I(t), I_{\mathrm{sat}}, k)$ has to be substituted back into eqn (9) before application of the nonlinear

Table 1 Nonlinear optical parameters obtained by employing the three-level diagram model, where eqn (1)–(3) (for complex **2** and **2-TF**) and (6)–(12) (for complexes **3a**, **3b**, **3a-TF** and **3b-TF**) were used for simulation at nanosecond regime

Complex	σ_{01} (cm^2)	σ_{23} (cm^2)	k	τ_{10} (ns)
2	$^{a}4.85 \times 10^{-18}$	—	$^{a}8.08$	$^{a}5.32$
2-TF	$^{a}1.62 \times 10^{-17}$	—	$^{a}19.3$	—
3a	2.36×10^{-17}	9.92×10^{-17}	4.20	5.40 (22)
3a-TF	1.89×10^{-17}	4.01×10^{-16}	21.2	—
3b	5.53×10^{-17}	2.72×10^{-16}	4.91	4.50 (27)
3b-TF	2.24×10^{-17}	6.92×10^{-16}	30.9	—

[a] Values obtained from ref. 39, τ_{ph} (μs) in brackets.

absorption coefficient to open-aperture *Z*-scan experimental data. At this stage, the possible integration over a homogeneous sample of thickness L leads to a transcendental equation for transmission T as $T = I_{out}/I_{in}$, derived as:[62]

$$T(F,k,F_{sat}) = \exp(-\alpha_0 L)\left(\frac{F_{sat}+kT(F,k,F_{sat})F}{F_{sat}+kF}\right)^{1-\frac{1}{k}} \quad (12)$$

The nonlinear optical parameters obtained by fitting the *Z*-scan experimental signatures of complex **2** and its respective thin film **2-TF**[39] are listed in Table 1.

The concentration of complexes **3a** and **3b** at 3.0×10^{-4} M or 1.869×10^{17} molecules per cm^3 has been selected to match that of complex **2**,[39] noting that due to saturation, the concentration of particles exceeded this value. This concentration selection creates fair comparison of nonlinear optical parameters for all complexes under investigation. These complexes showed no aggregation when concentration studies aimed at determining the molar extinction coefficients were performed. The open aperture *Z*-scan signatures of complexes **3a** and **3b** were more pronounced than those for complex **2** with **3b** being the best, Fig. 4A. This enhanced nonlinear behavior can be attributed to a more extensive π-conjugated system in complexes **3a** and **3a** (Fig. 4A) compared to that of complex **2** and is in agreement with the nonlinear behavior proposed for the extension of π-electron system and heavy lanthanide central metal.[57,63–65] Complexes **3a-TF** and **3b-TF** (Fig. 4C) exhibited better open aperture *Z*-scan signals that complexes **3a** and **3b**, respectively. This observation is similar to that of **2-TF** in comparison to complex **2**. The σ_{23} values for complexes **3a**, **3b**, **3a-TF** and **3b-TF** are shown in Table 1. The σ_{23} value is greater for the complex than for its respective thin film, evidencing the observed open aperture *Z*-scan signatures. It can also be observed that the σ_{01} values for **3a** and **3b** are larger than those for **3a-TF** and **3b-TF**, hence the larger k values of **3a-TF** and **3b-TF** in comparison to those of **3a** and **3b** but smaller than those of **2-TF** (Table 2). This observation can be attributed to the aggregation which may have directly affected the ground state and the excited state absorption cross sections of thin films in different ways. Similarly, the k values for complexes **3a** and **3b** are smaller than those for complex **2**.

The scanning electron microscopy (SEM) images of **2-TF**,[39] **3a-TF** and **3b-TF** were obtained for the samples on thin glass slides. These images were taken after performing the open aperture *Z*-scan experiments (discussed below) where the hazard of the laser beams pumped into the thin films could possibly result in holes and wrinkles on the surface as result of thermal effect. The SEM images of thin films were taken by focusing on the irradiated area (Fig. S6†). As can be seen in the SEM images (Fig. S6†), the surface exhibited homogeneity without any holes or pockets, proving that thin films were thermally stable.

3.3.1 Other nonlinear optical parameters.

Further analysis of the effective intensity dependent nonlinear absorption coefficient (β_{eff}) was carried out by employing the nonlinear regression technique to manipulate the open aperture *Z*-scan data. This was performed by employing eqn (13), in which the normalized transmittance ($T_{Norm}(z)$) is defined as a function of *z*-position, described by Sutherland *et al.*:[66]

$$T_{Norm}(z) = \frac{1}{\left[1+(n-1)\beta_{eff}L_{eff}\left(\frac{I_0}{1+\left(\frac{z}{z_0}\right)^2}\right)^{n-1}\right]^{\frac{1}{n-1}}}, \quad (13)$$

where I_0 (kept at 0.87 GW cm^{-2} throughout the experiment) is the intensity of the beam at focus for $n = 2$ for two photon absorption, respectively, and z and z_0 are the sample positions with respect to the input intensity and Rayleigh length, defined by $\frac{\pi {w_0}^2}{\lambda}$ (λ = wavelength of the laser beam and w_0 = beam waist ($\sim 2.56 \times 10^{-3}$ cm) at the focus ($z = 0$)), respectively. We have applied this model to complexes **2** and **2-TF**.[39] When using eqn (13), there is an assumption that the higher singlet excited-state absorption cross section contributes significantly to the reverse saturable absorption and, therefore, only applies to complex **2** and its thin film, which exhibit lack of triplet–triplet absorption. To accommodate optical limiters, the mechanisms of which are governed by strong triplet–triplet absorption at the nanosecond regime, the effective absorption coefficient can be calculated according to the previously reported theory.[67] The normalized transmittance in this case is defined by:

$$T_{Norm}(z) = \frac{\log_e\left(1+\frac{q_0(z)}{1+\frac{z^2}{{z_0}^2}}\right)}{\left(\frac{q_0(z)}{1+\frac{z^2}{{z_0}^2}}\right)}, \quad (14)$$

Table 2 Nonlinear optical parameters obtained by using the nonlinear regression technique at 532 nm for all complexes[a]

Complex	Im[$\chi^{(3)}$] (esu)	γ (esu)	I_{lim} (J cm^{-2})	Reduction of T_{Norm} (%)
2	3.77×10^{-10}	9.74×10^{-28}	—	48
2-TF	1.19×10^{-8}	3.07×10^{-26}	0.31	82
3a	2.00×10^{-9}	5.17×10^{-27}	0.34	66
3a-TF	9.82×10^{-9}	25.3×10^{-27}	0.10	82
3b	4.91×10^{-9}	12.7×10^{-27}	0.10	80
3b-TF	1.25×10^{-8}	32.2×10^{-27}	0.03	90

[a] — denotes that the I_{lim} value could not be determined due to less than 50% reduction in T_{Norm}.

$$q_0(z) = \frac{\sigma_{\text{ex}} F_0(r=0)\alpha L_{\text{eff}}}{2hv}, \tag{15}$$

where $F_0(r = 0)$ is the on-axis fluence at the focus.

Other theories[68,69] can, therefore, be applied to calculate the effective absorption coefficient. T_{Norm} is then given by:

$$T_{\text{Norm}}(z) = \frac{\text{Log}_\text{e}(1 + q_0(z))}{q_0(z)} \tag{16}$$

In this expression, $q_0(z)$ given by:

$$q_0(z) = \frac{\beta_{\text{eff}} I_0 L_{\text{eff}}}{1 + \dfrac{z^2}{{z_0}^2}} \tag{17}$$

In eqn (13), (15) and (17), L_{eff} is commonly described as the effective thickness of the sample given by

$$L_{\text{eff}} = \frac{1 - \text{e}^{-\alpha L}}{\alpha} \tag{18}$$

In eqn (18), α and L are the linear absorption coefficient and the thickness of the sample, respectively.

Once the β_{eff} values were obtained applying the nonlinear regression techniques, we could easily compute the proportionality third order optical susceptibility (Im[$\chi^{(3)}$] in esu), which is an imaginary component, *via* eqn (19):[70,71]

$$-\text{Im}\left[\chi^{(3)}\right] = \frac{\left({n_0}^2 \varepsilon_0 c \lambda \beta_{\text{eff}}\right)}{(2\pi)} \tag{19}$$

In eqn (19), c and n_0, respectively, are the speed of light in vacuum and the linear refractive index, ε_0 is the permittivity of free space and λ is the wavelength of the laser light.

At the molecular level, there is a direct correlation between Im[$\chi^{(3)}$] (in esu) and the hyperpolarizability γ (which provides the nonlinear absorption per mole of the sample), expressed by eqn (20):[71,72]

$$\gamma = \frac{\text{Im}\left[\chi^{(3)}\right]}{N^* f^4} \tag{20}$$

$N^* = C_{\text{mol}} N_\text{A}$ (C_{mol} is the concentration of the active species in the excited state in mol) and f denotes the Lorenz local field factor, given by eqn (21):

$$f = \frac{n^2 + 2}{3} \tag{21}$$

The optical limiting threshold is also very important to consider since it indicates the degree by which the transmission of the laser beam intensities to be received by an optical sensor being protected by an optical limiter is reduced. By definition, limiting intensity (I_{lim} in J cm^{-2}) is the incident fluence at which the output fluence is half (50%) of the linear transmission.[73,74] This refers to any strong attenuation, experienced by the photodiode detector when the nonlinear optical material responds to the intense beams. Such attenuations are an indication of an optical limiting effect. The I_{lim} values for complexes **2**,[39] **3a** and **3b** as well as **2-TF**,[39] **3a-TF** and **3b-TF** were, therefore, obtained at 50% of the linear transmittance by plotting the T_{Norm} (related to the output fluence) against the input fluence (Fig. 6).

As indicated before, complex **2** (ref. 39) exhibits a different nonlinear optical mechanism to that shown by complexes **3a** and **3b**. This makes it difficult to compare Im[$\chi^{(3)}$] and the γ values, calculated for these complexes. However, given the fact that complexes **3a** and **3b** were designed by sandwiching the Cd(II) ion between the complex **2** molecules, the change in the mechanism is still very interesting. Despite the challenge of comparing the *Z*-scan experimental data, the assumptions made when deriving eqn (1)–(3) and (6)–(8) help ignore other possible contributions made by S_m and T_3. This way, we can look at the pure processes that govern the nonlinear optical behavior observed for each complex. Although the behavior of complex **2** is based on two-photon absorption (2-PA) while for complex **3a** and **3b** on one-photon absorption (1-PA), the σ_{1m} and σ_{23} values should be comparable. The open-aperture *Z*-scan experimental data shows the trend: $\sigma_{23} \gg \sigma_{1m}$, with σ_{23} for complex **3b** greater than that of complex **3a**, hence the better open aperture *Z*-scan signatures for complexes **3a** and **3b** compared to complex **2**. The calculated Im[$\chi^{(3)}$] and γ values follow a similar trend, with those of complexes **3a** and **3b** (Table 2) being higher than those of complex **2**. For **2-TF**, the Im[$\chi^{(3)}$] and γ values (Table 2) were very high and larger than those of complex **2**, as discussed previously.[39] Similarly the Im[$\chi^{(3)}$] and γ values for **3a-TF** and **3b-TF** are greater than those calculated for complexes **3a** and **3b**. This observation is in agreement with what has been observed before.[42,75] However, the Im[$\chi^{(3)}$] and γ values for **3a-TF** were smaller than those of **2-TF**. This overturn in the observed pattern of the Im[$\chi^{(3)}$] and γ values is attributed to aggregation,[69] which is a known phenomenon in thin films that can affect the excited state absorption, thereby, deactivating the populated excited state. This observation is subjective since aggregation does not always exist in thin films, resulting in gigantic Im[$\chi^{(3)}$] and γ values.[39] Overall, the better nonlinear optical behavior observed for complexes **3a** and **3b** compared to that of complex **2** in solution is a good indication of the influence of the extension of π-electron system at the same

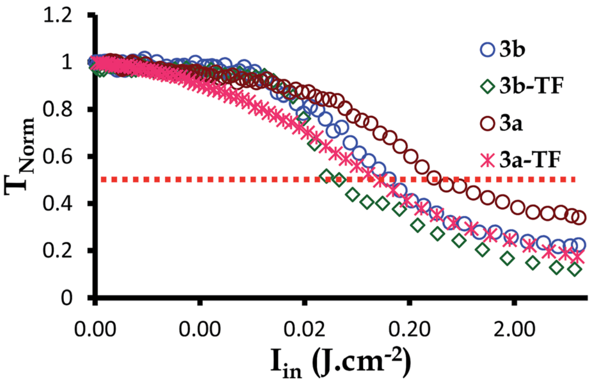

Fig. 6 The normalized transmittance against the incident intensity plot for complexes 3a and 3b as well as their respective thin films 3a-TF and 3b-TF at the nanosecond regime.

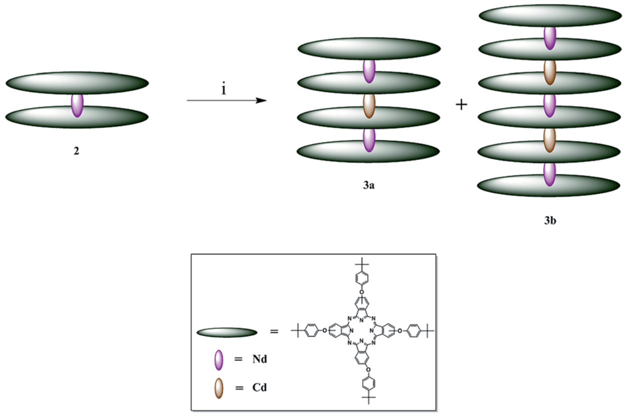

Scheme 1 Synthetic pathway to obtain complexes **3a** and **3b**; i = TCB and cadmium acetate dihydrate at reflux temperature, 24 h.

concentration. This is also evident when comparing complex **3a** to complex **3b**, with **3a** being the best optical limiter. The I_{lim} values were also analyzed. These values are meant to be minimal for an efficient optical limiter.

Complexes **3a** and **3b** reduced the T_{Norm} by more than 50%, hence the signals in Fig. 6 and the I_{lim} values in Table 2. The I_{lim} value is lower for complex **3b**, indicating that complex **3b** is a better optical limiter than complex **3a**. A similar behavior was observed for **3a-TF** and **3b-TF**, with **3b-TF** being a better optical limiter in solid state. In general, all thin films exhibited a reduction in T_{Norm} of greater than 90% and lower I_{lim} values than those in solution.

4. Conclusions

A rare type of new n-tuple decker phthalocyanines were investigated for optical limiting applications. The broad absorption spectra of complexes **3a** and **3b** exhibited larger ground state absorption cross sections, which compete with the triplet excited state absorption cross sections, resulting in the lowest k values for complexes **3a** and **3b** compared to that of complex **2**. It was also observed that the lack of interaction between the H_2Pc ligands of complexes **3a** and **3b** enhanced the triplet population, thus changing the NLO mechanisms that control the reverse saturable absorption. More importantly, the extension of the π-electron system results in enhanced open aperture Z-scan signatures, also evidenced by the large $\text{Im}[\chi^{(3)}]$ and γ values for complexes **3a** and **3b** compared to those of **2**.

Author contributions

The manuscript was written through contributions of all authors. All authors have given approval to the final version of the manuscript.

Funding sources

Department of Science and Technology (DST) and National Research Foundation (NRF).

Conflicts of interest

There are no conflicts of interest to declare.

Abbreviations

NLO	Nonlinear optical
DMF	Dimethyl formamide
DCM	Dichloromethane
DBU	1,8-Diazabicyclo[5.4.0]undec-7-ene
TCB	1,2,4-Trichlorobenzene
THF	Tetrahydrofuran
MS	Mass spectrum
NMR	Nuclear magnetic resonance
XTD	X-ray diffraction
UV-Vis	Ultraviolet-visible
TCSPC	Time correlated single photon counting
ESR	Electron spin resonance
SEM	Scanning electron microscope
$LnPc_2$	Lanthanide bisphthalocyanine
H_2Pc	Unmetallated phthalocyanine
BV	Blue valence
VEH	Valence-Effective Hamiltonian
RSA	Reverse saturable absorption
T_{Norm}	Normalized transmittance
ISC	Intersystem crossing
I_{lim}	Limiting threshold
2-PA	Two-photon absorption
1-PA	One-photon absorption

Acknowledgements

This study was supported by the Department of Science and Technology (DST) and National Research Foundation (NRF), South Africa, through DST/NRF South African Research Chairs Initiative for Professor of Medicinal Chemistry and Nanotechnology (UID 62620), NRF (UID 110789), and by Rhodes University.

References

1 J. Jiang and D. K. P. Ng, A Decade Journey in the Chemistry of Sandwich-Type Tetrapyrrolato-Rare Earth Complexes, *Acc. Chem. Res.*, 2009, **42**(1), 79–88.
2 M. Gonidec, I. Krivokapic, J. Vidal-Gancedo, E. S. Davies, J. McMaster, S. M. Gorun and J. Veciana, Highly Reduced Double-Decker Single-Molecule Magnets Exhibiting Slow Magnetic Relaxation, *Inorg. Chem.*, 2013, **52**, 4464–4471.
3 M. Gonidec, D. B. Amabilino and J. Veciana, Novel double-decker phthalocyaninato terbium(III) single molecule magnets with stabilised redox states, *Dalton Trans.*, 2012, **41**, 13632–13639.
4 H. Wang, B.-W. Wang, Y. Bian, S. Gao and J. Jiang, Single-molecule magnetism of tetrapyrrole lanthanide compounds with sandwich multiple-decker structures, *Coord. Chem. Rev.*, 2016, **306**, 195–216.

5 M. Mannini, F. Bertani, C. Tudisco, L. Malavolti, L. Poggini, K. Misztal, D. Menozzi, A. Motta, E. Otero, P. Ohresser, P. Sainctavi, G. G. Condorelli, E. Dalcanale and R. Sessoli, Magnetic behaviour of TbPc2 single-molecule magnets chemically grafted on silicon surface, *Nat. Commun.*, 2014, **5**, 4582.

6 T. Fukuda, W. Kuroda and N. Ishikawa, Observation of long-range f–f interactions between two f-electronic systems in quadruple-decker phthalocyanines, *Chem. Commun.*, 2011, **47**, 11686–11688.

7 S. Lee and T. Ogawa, Molecular Design for Single-molecule Magnetism of Lanthanide Complexes, *Chem. Lett.*, 2017, **46**, 10–18.

8 H. Shang, S. Zeng, H. Wang, J. Dou and J. Jiang, Peripheral Substitution: An Easy Way to Tuning the Magnetic Behavior of Tetrakis(phthalocyaninato) Dysprosium(III) SMMs, *Sci. Rep.*, 2015, **5**, 8838.

9 H. Wang, K. Qian, D. Qi, W. Cao, K. Wang, S. Gao and J. Jiang, Co-crystallized fullerene and a mixed (phthalocyaninato)(porphyrinato) dysprosium double-decker SMM, *Chem. Sci.*, 2014, **5**, 3214–3220.

10 H. Wang, K. Wang, J. Tao and J. Jiang, Twist angle perturbation on mixed (phthalocyaninato)(porphyrinato) dysprosium(III) double-decker SMMs, *Chem. Commun.*, 2012, **48**, 2973–2975.

11 D. Xie, W. Pan, Y. D. Jiang and Y. R. Li, Erbium bis [phthalocyaninato] complex LB film gas sensor, *Mater. Lett.*, 2003, **57**(16–17), 2395–2398.

12 T. Basova, I. Jushina, A. G. Gürek, V. Ahsen and A. K. Ray, Use of the electrochromic behaviour of lanthanide phthalocyanine films for nicotinamide adenine dinucleotide detection, *J. R. Soc., Interface*, 2008, **5**(24), 801–806.

13 M. G. Martín, M. L. Rodríguez-Méndez and J. A. de Saja, Films of Lutetium Bisphthalocyanine Nanowires As Electrochemical Sensors, *Langmuir*, 2010, **26**(24), 19217–19224.

14 J. Padilla and W. E. Hatfield, Correlation between π-orbital overlap and conductivity in bis-phthalocyaninato lanthanides, *Inorg. Chim. Acta*, 1991, **185**(2), 131–136.

15 R. Jones, A. Krier and K. Davidson, Structure, electrical conductivity and electrochromism in thin films of substituted and unsubstituted lanthanide bisphthalocyanines, *Thin Solid Films*, 1997, **298**(1–2), 228–236.

16 W. Göpel, Phthalocyanine prototype interfaces: Their importance for designing chemical sensor and molecular electronic devices, *Synth. Met.*, 1991, **41**(3), 1087–1093.

17 W. Cao, H. Wang, X. Wang, H. K. Lee, D. K. P. Ng and J. Jiang, Constructing Sandwich-Type Rare Earth Double-Decker Complexes with N-Confused Porphyrinato and Phthalocyaninato Ligands, *Inorg. Chem.*, 2012, **51**, 9265–9272.

18 K. E. Sekhosana and T. Nyokong, Synthesis of ytterbium bisphthalocyanines: Photophysicochemical properties and nonlinear absorption behavior, *Opt. Mater.*, 2014, **37**, 139–146.

19 K. E. Sekhosana, M. H. Manyeruke and T. Nyokong, Synthesis and optical limiting properties of new lanthanide bis- and tris-phthalocyanines, *J. Mol. Struct.*, 2016, **1121**, 111–118.

20 A. I. Plekhanov, T. V. Basova, R. G. Parkhomenko and A. G. Gürek, Nonlinear optical properties of lutetium and dysprosium bisphthalocyanines at 1550 nm with femto- and nanosecond pulse excitation, *Opt. Mater.*, 2017, **64**, 13–17.

21 L.-C. Liu, C.-H. Tai, A. T. Hu and T.-H. Wei, Nonlinear optical properties of lutetium bisphthalocyanine and its application for an optical switch, *J. Porphyrins Phthalocyanines*, 2004, **8**(7), 984–988.

22 S. Saydam, E. Yılmaz, F. Bağcı, H. G. Yağlioğlu, A. Elmalı, B. Salih and Ö. Berkaroğlu, Synthesis, characterization and electrochemical and optical limiting properties of novel CoII, CuII and double-decker LuIII phthalocyanines, *Eur. J. Inorg. Chem.*, 2009, **14**, 2096–2103.

23 M. M. Ayhan, A. Singh, C. Hirel, A. G. Gürek, V. Ahsen, E. Jeanneau, I. Ledoux-Rak, J. Zyss, C. Andraud and Y. Bretonnière, ABAB homoleptic bis (phthalocyaninato) lutetium (III) complex: toward the real octupolar cube and giant quadratic hyperpolarizability, *J. Am. Chem. Soc.*, 2012, **134**(8), 3655–3658.

24 B. Ren, N. Sheng, B. Gu, Y. Wan, G. Rui, C. Lv and Y. Cui, Changing optical nonlinearities of homoleptic bis(phthalocyaninato) rare earth praseodymium double-decker complexes by the redox reaction, *Dyes Pigm.*, 2017, **139**, 788–794.

25 A. B. Karpo, V. E. Pushkarev, V. I. Krasovskii and L. G. Tomilova, Z-scan study of nonlinear absorption in novel lanthanide bis-phthalocyanines, *Chem. Phys. Lett.*, 2012, **554**, 155–158.

26 K. E. Sekhosana, M. Shumba and T. Nyokong, Electrochemical and non-linear optical behavior of a new neodymium double-decker phthalocyanine, *Polyhedron*, 2017, **138**, 154–160.

27 N. Sheng, D. Liu, B. Gu, J. He and Y. Cui, A series of homoleptic bis(phthalocyaninato) rare earth sandwich complexes with large two-photon absorption cross-section, *Dyes Pigm.*, 2015, **122**, 346–350.

28 N. Sheng, Z. Yuan, J. Wang, W. Chen, J. Sun and Y. Bian, Third-order nonlinear optical properties of sandwich-type mixed (phthalocyaninato)(porphyrinato) europium double- and triple-decker complexes, *Dyes Pigm.*, 2012, **95**, 627–631.

29 J. Kan, Y. Chen, D. Qi, Y. Liu and J. Jiang, High-Performance Air-Stable Ambipolar Organic Field-Effect Transistor Based on Tris(phthalocyaninato) Europium(III), *Adv. Mater.*, 2012, **24**, 1755–1758.

30 Y. Chen, W. Su, M. Bai, J. Jiang, X. Li, Y. Liu, L. Wang and S. Wang, High Performance Organic Field-Effect Transistors Based on Amphiphilic Tris(phthalocyaninato) Rare Earth Triple-Decker Complexes, *J. Am. Chem. Soc.*, 2005, **127**, 15700–15701.

31 M. Urdampilleta, S. Klyatskaya, J.-P. Cleuziou, M. Ruben and W. Wernsdorfer, Supramolecular spin valves, *Nat. Mater.*, 2011, **10**, 502–506.

32 R. Sun, L. Wang, J. Tian, X. Zhang and J. Jiang, Self-assembled nanostructures of optically active phthalocyanine derivatives. Effect of central metal ion on the morphology, dimension, and handedness, *Nanoscale*, 2012, **4**, 6990–6996.

33 G. Lu, Y. Chen, Y. Zhang, M. Bao, Y. Bian, X. Li and J. Jiang, Morphology Controlled Self-Assembled Nanostructures of Sandwich Mixed (Phthalocyaninato)(Porphyrinato) Europium Triple-Deckers. Effect of Hydrogen Bonding on Tuning the Intermolecular Interaction, *J. Am. Chem. Soc.*, 2008, **130**, 11623–11630.

34 N. Kılınç, D. Atilla, A. G. Gürek, Z. Z. Öztürk and V. Ahsen, Volatile organic compounds sensing properties of tetrakis(alkylthio)-substituted lutetium(III) bisphthalocyanines thin films, *Talanta*, 2009, **80**, 263–268.

35 P. Zhu, Y. Wang, M. Ren, X. Zhao and X. Zhang, Sandwich-type heteroleptic tris(phthalocyaninato) terbium triple-decker: Single crystal structure and self-assembled nanostructures, *Inorg. Chim. Acta*, 2012, **392**, 10–15.

36 T. Fukuda, T. Biyajima and N. Kobayashi, A Discrete Quadruple-Decker Phthalocyanine, *J. Am. Chem. Soc.*, 2010, **132**, 6278–6279.

37 H. Wang, N. Kobayashi and J. Jiang, New Sandwich-Type Phthalocyaninato–Metal Quintuple-Decker Complexes, *Chem.–Eur. J.*, 2012, **18**, 1047–1049.

38 H. Wang, D. Qi, Z. Xie, W. Cao, K. Wang, H. Shang and J. Jiang, A sandwich-type phthalocyaninato metal sextuple-decker complex: synthesis and NLO properties, *Chem. Commun.*, 2013, **49**, 889–891.

39 K. E. Sekhosana, R. Nkhahle and T. Nyokong, The Primary Demonstration of Exciton Coupling Effects on Optical Limiting Properties of Blue Double-Decker Lanthanide Phthalocyanine Salts, *ChemistrySelect*, 2018, **3**, 6671–6682.

40 K. E. Sekhosana, E. Antunes, S. Khene, S. D'Souza and T. Nyokong, Fluorescence behavior of glutathione capped CdTe@ZnS quantum dots chemically coordinated to zinc octacarboxy phthalocyanines, *J. Lumin.*, 2013, **136**, 255–264.

41 K. E. Sekhosana, E. Antunes and T. Nyokong, Glutathione capped CdTe@ZnS quantum dots–zinc tetracarboxy phthalocyanine conjugates: Fluorescence behavior studies in comparison with zinc octacarboxy phthalocyanine, *Polyhedron*, 2013, **54**, 294–299.

42 K. E. Sekhosana and T. Nyokong, The nonlinear absorption in new lanthanide double decker pyridinebased phthalocyanines in solution and thin films, *Opt. Mater.*, 2015, **47**, 211–218.

43 H. Shang, H. Wang, W. Li and J. Jiang, Vibrational spectroscopy of phthalocyanine and naphthalocyanine in sandwich-type (na)phthalocyaninato and porphyrinato rare earth complexes. Part 15: The IR characteristics of phthalocyanine in homoleptic tetrakis(phthalocyaninato) rare earth(III)-cadmium(II) quadruple-deckers, *Vib. Spectrosc.*, 2013, **69**, 8–12.

44 E. Orti and J.-L. Brédas, Photoelectron Spectra of Phthalocyanine Thin Films: A Valence Band Theoretical Interpretation, *J. Am. Chem. Soc.*, 1992, **114**(22), 8669–8675.

45 V. Lemaur, M. Steel, D. Beljonne, D. Brédas and J.-L. Cornil, Photoinduced Charge Generation and Recombination Dynamics in Model Donor/Acceptor Pairs for Organic Solar Cell Applications: A Full Quantum-Chemical Treatment, *J. Am. Chem. Soc.*, 2005, **127**(16), 6077–6088.

46 T. C. VanCott, Z. Gasyna, P. N. Schatz and M. E. Boyle, Magnetic circular dichroism and absorption spectra of lutetium bis(phthalocyanine) isolated in an argon matrix, *J. Phys. Chem.*, 1995, **99**(13), 4820–4830.

47 C. Dunfold, B. Williamson and E. Krausz, Temperature-Dependent Magnetic Circular Dichroism of Lutetium Bisphthalocyanine, *J. Phys. Chem. A*, 2000, **104**(16), 3537–3543.

48 N. Ishikawa, O. Ohno and Y. Kaizu, Electronic states of bis(phthalocyaninato)lutetium radical and its related compounds: the application of localized orbital basis set to open-shell phthalocyanine dimers, *J. Phys. Chem.*, 1993, **97**(5), 1004–1010.

49 N. Ishikawa and Y. Kaizu, Disappearance of MCD A term in the fingerprint band of cation radicals of phthalocyanine metal complexes, *Chem. Phys. Lett.*, 2001, **339**(1–2), 125–132.

50 N. Ishikawa, O. Ohno, Y. Kaizu and H. Kobayashi, Localized orbital study on the electronic structure of phthalocyanine dimers, *J. Phys. Chem.*, 1992, **96**(22), 8832–8839.

51 M. Calvete, G. Y. Yang and M. Hanack, Porphyrins and phthalocyanines as materials for optical limiting, *Synth. Met.*, 2004, **141**(3), 231–243.

52 C. R. Mendonça, L. Gaffo, L. Misoguti, W. C. Moreira, O. N. Oliveira and S. C. Zilio, Characterization of dynamic optical nonlinearities in ytterbium bis-phthalocyanine solution, *Chem. Phys. Lett.*, 2000, **323**(3–4), 300–304.

53 E. Orti, J. L. Bredas and C. Clarisse, Electronic structure of phthalocyanines: theoretical investigation of the optical properties of phthalocyanine monomers, dimers, and crystals, *J. Chem. Phys.*, 1990, **92**(2), 1228–1235.

54 M. Kandaz, A. T. Bilgiçli and A. Altındal, Metal ion sensing functional mono and double-decker lanthanide phthalocyanines: Synthesis, characterization and electrical properties, *Synth. Met.*, 2010, **160**(1–2), 52–60.

55 K. E. Sekhosana, E. Amuhaya and T. Nyokong, Nonlinear optical behavior of neodymium mono- and bi-nuclear phthalocyanines linked to zinc oxide nanoparticles and incorporated into poly acrylic acid, *Polyhedron*, 2016, **105**, 159–169.

56 S. Sapra and D. D. Sarma, Simultaneous control of nanocrystal size and nanocrystal-nanocrystal separation in CdS nanocrystal assembly, *Pramana*, 2005, **65**(4), 565–570.

57 L. De Boni, L. Gaffo, L. Misoguti and C. R. Mendonça, Nonlinear absorption spectrum of ytterbium bis-phthalocyanine solution measured by white-light continuum Z-scan technique, *Chem. Phys. Lett.*, 2006, **419**(4–6), 417–420.

58 M. G. Vivas, E. G. R. Fernandes, M. L. Rodríguez-Méndez and C. R. Mendonca, Study of singlet excited state absorption spectrum of lutetium bisphthalocyanine using the femtosecond Z-scan technique, *Chem. Phys. Lett.*, 2012, **531**, 173–176.

59 S. M. O'Flahery, S. V. Hold, M. J. Cook, T. Torres, Y. Chen, M. Hanack and W. J. Blau, Molecular Engineering of Peripherally and Axially Modified Phthalocyanines for Optical Limiting and Nonlinear Optics, *Adv. Mater.*, 2003, **15**(1), 19–32.

60 M. Yüksek, A. Elmali, M. Durmuş, H. G. Yağlioğlu, H. Ünver and T. Nyokong, Good optical limiting performance of indium and gallium phthalocyanines in a solution and co-polymer host, *J. Opt.*, 2010, **12**(1), 015208 (9 pages).

61 J. S. Shirk, R. G. S. Pong, R. S. Flom, H. Heckmann and M. Hanack, Effect of Axial Substitution on the Optical Limiting Properties of Indium Phthalocyanines, *J. Phys. Chem. A*, 2000, **104**(7), 1438–1449.

62 S. M. O'Flaherty, J. J. Doyle and W. J. Blau, Numerical Approach for Optically Limited Pulse Transmission in Polymer-Phthalocyanine Composite Systems, *J. Phys. Chem. B*, 2004, **108**, 17313–17319.

63 L. Chen, R. Hu, J. Xu, S. Wang, X. Li, S. Li and G. Yang, Third-order nonlinear optical properties of a series of porphyrin-appended europium(III) bis(phthalocyaninato) complexes, *Spectrochim. Acta, Part A*, 2013, **105**, 577–581.

64 R. Rousseau, R. Aroca and M. L. Rodríguez-Méndez, Extended Hückel molecular orbital model for lanthanide bisphthalocyanine complexs, *J. Mol. Struct.*, 1995, **356**, 49–62.

65 M. J. F. Calvete, D. Dini, S. R. Flom, M. Hanack, R. G. S. Pong and J. S. Shirk, Synthesis of a Bisphthalocyanine and its Nonlinear Optical properties, *Eur. J. Org. Chem.*, 2005, **16**, 3499–3509.

66 R. L. Sutherland, *Handbook of Nonlinear Optics, Second Edition, Revised and expanded*, Marcel Dekker, New York, NY, 2003.

67 G. L. Wood, M. J. Miller and A. G. Mott, Investigation of tetrabenzporphyrin by the Z-scan technique, *Opt. Lett.*, 1995, **20**(9), 973–975.

68 M. Sheik-Bahae, A. A. Said, T.-H. Wei, D. J. Hagan and E. W. Van Stryland, Sensitive measurement of optical nonlinearities using a single beam, *IEEE J. Quantum Electron.*, 1990, **26**, 760–769.

69 C. H. Kwak, Y. L. Lee and S. G. Kim, Analysis of asymmetric Z-scan measurement for large optical nonlinearities in an amorphous As2S3 thin film, *J. Opt. Soc. Am. B*, 1999, **16**(4), 600–604.

70 P. Zhao, S. Xu, Z. Y. Li and F.-S. Zhang, Nonlinear Optical Properties of Novel Polymeric Rare Earth Phthalocyanine Studied Using Picosecond Z-Scan Technique, *Chin. Phys. Lett.*, 2008, **25**(6), 2058–2061.

71 Y. Chen, M. Hanack, Y. Araki and O. Ito, Axially modified gallium phthalocyanines and naphthalocyanines for optical limiting, *Chem. Soc. Rev.*, 2005, **34**(6), 517–529.

72 D. Dini and M. Hanack, in *The Porphyrin Handbook: Physical Properties of Phthalocyane-based Materials*, ed. K. M. Kadish, K. M. Smith and R. Guilard, Academic Press, USA, 2003, vol. 17, p. 22.

73 S. V. Rao, Femtosecond and continuous-wave nonlinear optical properties of (H2)2SnPc, $Sn(OH)_2Pc$, and $Sn(Cl)_2Pc$ studied using Z-scan technique, *Proc. SPIE*, 2009, **7197**, 719715.

74 Y. Chen, L. Gao, M. Feng, L. Gu, N. He, J. Wang, Y. Araki, W. J. Blau and O. Ito, Photophysical and Optical Limiting Properties of Axially Modified Phthalocyanines, *Mini-Rev. Org. Chem.*, 2009, **6**(1), 55–65.

75 K. E. Sekhosana and T. Nyokong, The optical limiting of blue and green ytterbium double-decker phthalocyanines in solution and in poly(acrylic acid) as thin films, *Inorg. Chim. Acta*, 2016, **450**, 87–91.